Proton transfer and tautomerism in 2-aminopurine–thymine and pyrrolocytosine–guanine base pairs

*Graham D. Bull and Katherine C. Thompson**

Department of Biological Sciences and Institute of Structural and Molecular Biology, Birkbeck, University of London, Malet Street, Bloomsbury, London WC1E 7HX

ABSTRACT: Pyrrolocytosine (PC) and 2-aminopurine (2AP) are fluorescent nucleobase analogues of the DNA nucleobases cytosine and adenine, respectively, and form base pairs with guanine and thymine. Both fluorescent nucleobases are used extensively as probes for local structure in nucleic acids as the fluorescence properties of PC and 2AP are very sensitive to changes such as helix formation, although the reasons for this sensitively are not clear. To address this question *ab initio* calculations have been used to calculate energies, at the MP2 and CIS level, of three different tautomer pairings of PC-G, and two of 2AP-T, which can potentially be interconverted by double proton transfer between the bases. Potential energy curves linking the different tautomer pairs have been calculated. For both PC-G and 2AP-T the most stable tautomer pair in the electronic ground state is that analogous to the natural C-G and A-T base pair. In the case of 2AP-T an alternative, stable, tautomer base pair was located in the first electronically excited state, however, it lies higher in energy than the tautomer pair analogous to A-T, making conversion to the alternative form

unlikely. In contrast, in the case of PC-G, an alternative tautomer base pair is found to be the most stable form in the first electronically excited state and this form is accessible following initial excitation from the ground state tautomer pair, thus suggesting an alternative deactivation route via double proton transfer may be possible when PC is involved in hydrogen bonding, such as occurs in helical conformations.

INTRODUCTION

The photochemical properties of molecules very similar to the natural DNA nucleobases, including tautomers of the bases, are often significantly different to those of the DNA nucleobases themselves.[1] The natural DNA nucleobases all have low fluorescence quantum yield and very short fluorescent decay times.[2] Fluorescent nucleobase analogues are structurally similar to the natural bases, and are often able to form Watson-Crick like base pairs with the natural DNA bases, but have enhanced fluorescent properties i.e. higher quantum yields and longer lifetimes under prevailing physiological conditions (e.g. pH and salinity). Variations in intra or intermolecular interactions, solvent exposure or pH changes, may lead to changes in fluorescence properties such as emission intensity, excitation intensity, or fluorescence lifetime of the probe.[3] For this reason fluorescent nucleobase analogues are extensively used as tools by experimentalists working with nucleic acids to study a wide range of biochemical questions both in vitro and more recently in vivo, examples of which are given in the recent review article by Xu *et al*.[4] A better understanding of the underlying physical basis for the change in fluorescence properties in different environments is required so that existing nucleobase analogues may be used more effectively and novel ones designed.

As early as 1969, Ward *et al*. reported that 2-aminopurine, a structural isomer of the base adenine (6-aminopurine), was highly fluorescent and could be selectively excited in the presence of natural nucleobases.[5] When 2-aminopurine is substituted for adenine it leads to minimal perturbation to the structure of the nucleic acid as both bases are structurally similar and both can form a Watson-Crick-like base pair with thymine in DNA and uracil in RNA.[6,7] As an example of this lack of structural perturbation, the 2-aminopurine containing oligodeoxynucleotide d(CTGA[2AP]TTCAG)$_2$ is still recognized and cleaved by the enzyme *Eco*RI endonuclease.[8] 2-Aminopurine can also substitute for guanine and form a wobble structure with cytosine,[6] which is the basis of mutagenicity of

2-aminopurine.[3,9] The left hand structure in Scheme 1, labeled 2AP–T TpI, ,where Tp stands for Tautomer pair, shows the bonding of 2AP and thymine in an analogous manner to the Watson-Crick hydrogen bonding that occurs between adenine and thymine in DNA. The structure on the right hand side, labeled 2AP–T TpII, shows an alternative scheme where although the overall geometry is effectively unchanged, the hydrogen bonding is between different tautomers of both 2AP and thymine which may be formed following proton or hydrogen exchange between the bases.

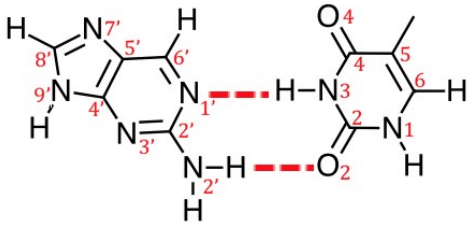

2-Aminopurine Thymine

2AP-T TpI

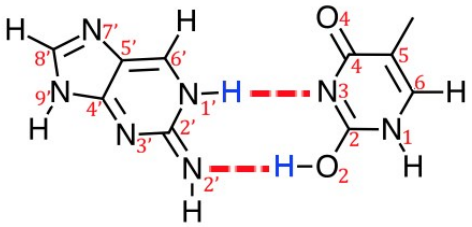

2-Aminopurine Thymine

2AP-T TpII

SCHEME 1: Chemical structures of the 2-aminopurine-thymine base pair. The structure on the left, 2AP–T TpI, is analogous to that of the adenine-thymine base pair commonly found in DNA, the structure on the right, 2AP–T TpII, is an alternative hydrogen bonding scheme involving different tautomers of both 2-aminopurine and thymine that may be formed by exchange of protons within the base pair.

The free base 2-aminopurine (2AP) itself has two major tautomers, 9H–2AP and 7H–2AP which exist in water with a 60% : 40% ratio, respectively,[10] however incorporation of 2AP into DNA fixes it in the 9H- tautomeric form. The electronic properties of 2AP are an excitation maximum of 305 nm that is red-shifted compared to adenine,[11] which has an excitation maximum at a wavelength of 260.5 nm.[12] The excited-state lifetimes (τ) of 2-aminopurine and 2-aminopurine riboside in an aqueous

environment (pH = 7) are 11.8 ns and 10.4 ns, respectively, with a fluorescence quantum yield (ϕ_f) of 0.66 and 0.65, respectively.[13] These values are significantly higher than for the natural DNA bases. However, when 2-aminopurine is incorporated into a single strand of DNA or RNA its fluorescence is quenched, and the fluorescence of 2AP is quenched further still upon formation of a DNA duplex or a DNA:RNA hybrid.[3] It is the sensitivity of 2-aminopurine to base sequence, temperature and helix conformation that enables its use to experimentalists as a fluorescent marker.[14, 15] The low energy absorption maximum of 2AP allows selective and direct excitation when it is incorporated within a synthetic DNA sequence. 2-Aminopurine has been used in numerous and diverse investigations including, as examples: as a marker for microRNA,[16] promoter structure,[17] a sodium ion aptamer,[18] DNA solvation,[19] structural dynamics within DNA[20-22] and protein induced conformational changes.[8,23,24]

Pyrrolocytosine is an analogue of the natural nucleobase cytosine and can form a pseudo Watson-Crick base pair with guanine, as shown in scheme 2.[25] Pyrrolocytosine (PC) has an excitation maximum at a wavelength of 345 nm[25] that is red-shifted compared to cytosine which is excited at a wavelength of 267 nm,[12] and hence may be selectively excited in the presence of the natural nucleobases. The usefulness of pyrrolocytosine is that, like 2AP, the fluorescence quantum yield of pyrrolocytosine is sensitive to the local environment of the nucleic acid in the region in which it is inserted. Tinsley and Walter quantified the extent of fluorescence quenching of pyrrolocytosine inserted into the middle of a single strand of RNA consisting of 20 additional bases, which was also combined with a complementary strand of RNA to form a duplex RNA hairpin.[26] It was found that the steady-state fluorescence of pyrrolocytosine was reduced by ~60% in the single strand RNA and by ~75% in the duplex RNA structure. Pyrrolocytosine has also found application in the study of structure and conformational changes in DNA,[27-29] metal-ion-mediated hybridization of oligonucleotides,[30] base flipping of pyrimidines,[31] investigation of DNA lesions,[32] transcription factor binding[33] and in the design of peptide nucleic acids.[34,35] Scheme 2 shows the expected structure of

pyrrolocytosine-guanine base pair (PC–G TpI), based on the hydrogen bonding in the cytosine-guanine base pair. Alternative base pairing can be envisaged involving different tautomeric forms of both pyrrolocytosine and guanine that may be formed by proton transfer within the base pair, these alternative tautomeric pairs are also shown in scheme 2, PC–G TpII and PC–G TpIII.

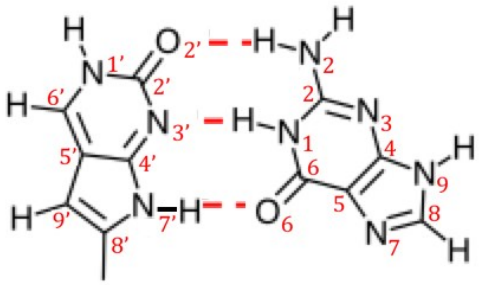

Pyrrolocytosine Guanine

PC–G TpI

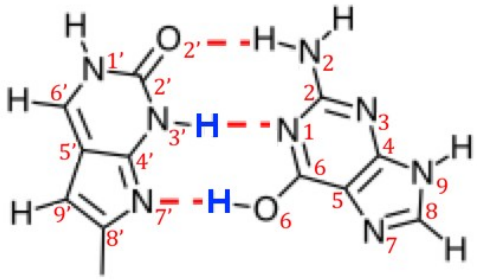

Pyrrolocytosine Guanine

PC–G TpII

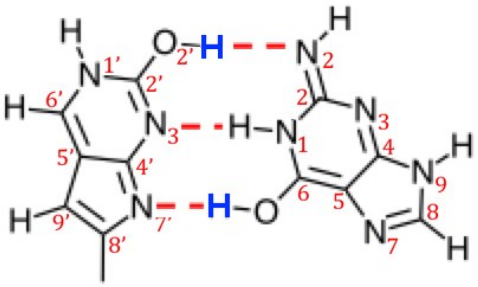

Pyrrolocytosine Guanine

PC–G TpIII

SCHEME 2: Chemical structures of the pyrrolocytosine-guanine base pair. The upper structure, PC–G TpI, is analogous to that of the cytosine-guanine base pair commonly found in DNA, the lower structures, PC–G TpII and PC–G TpIII, are alternative hydrogen bonding schemes involving different tautomers of both pyrrolocytosine and guanine that may be formed by exchange of protons within the base pair.

The reasons why the fluorescence of PC and 2AP are quenched in different environments are still not fully understood but such knowledge would both increase their utility to experimentalists and aid in understanding the properties, and reasons for the ultimate selection of the natural nucleobases during evolution. Although there have been numerous publications on the electronic

properties of the individual, and base stacked, nucleobase analogues pyrrolocytosine and 2-aminopurine,[e.g 15, 36-40] in the present study we have explored the electronic properties of the base pair systems, PG–G and 2AP–T, in particular the different tautomeric forms possible in the base paired systems, and how they may interconvert, considering both the electronic ground state, and electronically excited states. Equilibrium structures for PC–G and 2AP–T base pair tautomers formed as a result of double proton transfer are identified for the ground state (S_0) and the first electronic excited state (S_1). Potential energy curves for the electronic ground state (S_0), the electronic first excited state (S_1) and the $S_0 \rightarrow S_1$ vertical transition are mapped for the transfer of the $N_{3'}$–(H)N_1, $N_{7'}$(H)–O_6 and $O_{2'}$–(H)N_2 protons of the pyrrolocytosine-guanine (PC–G) base pair, and for the $N_{1'}$–(H)N_3 and $N_{2'}$(H)–O_2 protons of the 2-aminopurine-thymine (2AP–T) base pair. Examination of the dipole moment curves for the systems as the protons are transferred are also presented to provide more detail on how the electronic nature of the base pair changes during double proton transfer leading to the formation of the alternative tautomeric pairings.

MATERIALS AND METHODS

The ground state (S_0) geometry of the TpI pyrrolocytosine-guanine base pair was optimised at MP2/cc-pVDZ level using an input geometry taken from Thompson and Myake,[41] to produce structure TpI_{equi}. Optimized geometries of the other tautomer pairs, $TpII_{equi}$ and $TpIII_{equi}$, were similarly produced after exchange of the relevant protons. There are three protons shared between pyrrolocytosine and guanine in the PC–G base pair. Double proton transfer can take place between $N_{3'}$–(H)N_1 and $N_{7'}$(H)–O_6 sites and also between $O_{2'}$–(H)N_2 and $N_{7'}$(H)–O_6 sites (Scheme 2). Each of the potential energy curves for the H_1, $H_{7'}$ and H_2 proton migrations were constructed by optimising the structure but with the appropriate N–H bond length frozen in increasing 0.1 – 0.2 Å steps up to a maximum bond length of 2.4 Å. All other molecular coordinates were allowed to relax during geometry optimisation and no symmetry constraints were imposed.

The initial geometries for 2-aminopurine-thymine base pair used in this work were taken from Hardman and Thompson[15] and optimised as before. 2-Aminopurine-thymine have two protons that can be exchanged between the bases, $N_{1'}$–(H)N_3 and $N_{2'}$(H)–O_2 (Scheme 1). As was the case for the pyrrolocytosine-guanine base pair, the H_3 and $H_{2'}$ proton transfers of 2-aminopurine-thymine potential energy curves were constructed by freezing the appropriate N–H bond length in increasing 0.1 – 0.2 Å steps up to a maximum of 2.4 Å, and again all other molecular coordinates were allowed to relax during optimisation.

Vertical transition energies were calculated to construct potential energy curves for the $S_0 \rightarrow S_1$ transition as a function of the relevant proton position. The optimised geometries of the first excited state (S_1) were also calculated to define potential energy curves for each of the PC–G and 2AP–T proton transfers. In addition the geometries of the first three excited states (S_1, S_2 and S_3) of each of the tautomer base pairs considered were also determined. All excited state calculations were performed at the CIS/cc-pVDZ level. The CIS method was selected, rather than time dependent density function methods, TD-DFT, which are of comparable computational cost, because we wished to avoid problems associated with poorly represented charge transfer states between the nucleobases in the base pairs, the energies of which are underestimated by conventional TD-DFT methods, and may be either over or under estimated with long range corrected TD-DFT methods.[15, 42, 43]

MP2 optimised ground state geometries were used as input structures for the excited state calculations. No scaling has been applied to the vertical transition energies or oscillator strengths calculated using the CIS method (unless otherwise stated). To compare the transition energies for the $\pi \rightarrow \pi^*$ transitions to values in the literature readers may wish to apply a factor of 0.72 as recommended by Broo and Holmén[43] for these states. All calculations for this study were carried out using the Gaussian 03 suite of programs and Molekel was used to visualize molecular geometries and molecular orbitals.[44,45]

RESULTS AND DISCUSSION

The results presented in this section for the pyrrolocytosine-guanine and 2-aminopurine-thymine base pairs are from gas phase calculations only. Calculations using the PCM solvation model[46,47] gave qualitatively similar results to the gas phase calculations and are presented in the supplementary information. The results of the geometry optimizations presented below were performed without Counterpoise correction. To estimate the effect of basis set superposition error structures for which optimized geometries were located in the ground electronic state were re-optimised including Counterpoise correction, the results reveal marginally longer, <7%, hydrogen bond lengths in all cases.

Equilibrium Structures of Ground state Pyrrolocytosine-Guanine Tautomers

Possible base pair tautomers for PC–G are shown in Scheme 2. The tautomer PC–G TpI is analogous to the Watson-Crick guanine-cytosine base pair, whereas PC–G TpII could potentially be formed by the double proton transfer between $N_{3'}$–(H)N_1 and $N_{7'}$(H)–$O_{6'}$ and PC–G TpIII by the double proton transfer between $O_{2'}$–(H)N_2 and $N_{7'}$(H)–O_6. Optimisation of initial structures to find PC–G TpI_{equi} and PC–G $TpII_{equi}$ were successful and showed that PC–G TpI_{equi} is the more stable tautomer pair, with PC–G $TpII_{equi}$ lying +7.20 kcal mol^{-1} higher in energy. Attempts to find an equilibrium structure of PC–G TpIII were not successful, as the system moved back to PC–G TpI_{equi} each time. It will be shown later that this is not unexpected as any minimum for PC–G $TpIII_{equi}$ is at higher energy than PC–G TpI_{equi} and the minimum would be very shallow. The structures of PC–G TpI_{equi} and PC–G $TpII_{equi}$ are shown in Figure 1. In PC–G TpI_{equi} the ring systems were found to be C_s-

symmetric. This is in contrast to the C-G base pair which, when optimised at the same level, gives a structure where the amino group of guanine show significant pyramidization ($H_{2(}$-N_2-C_2-H_1 dihedral is 25°) although the hydrogen bond lengths are all similar (within 0.02 Å of the PC-G TpI_{equi} structure) and the interaction energy is only slightly smaller (by 2 kcal mol^{-1}). In PC–G $TpII_{equi}$ a slightly propeller twisted structure is found, which is caused by pyramidization of the amino group of guanine, with a $C_{2'}C_{4'}C_6C_2$ dihedral angle between the two bases of −5.7°. The three hydrogen bonds between PC and G are all approximately linear (within 10° of 180°).

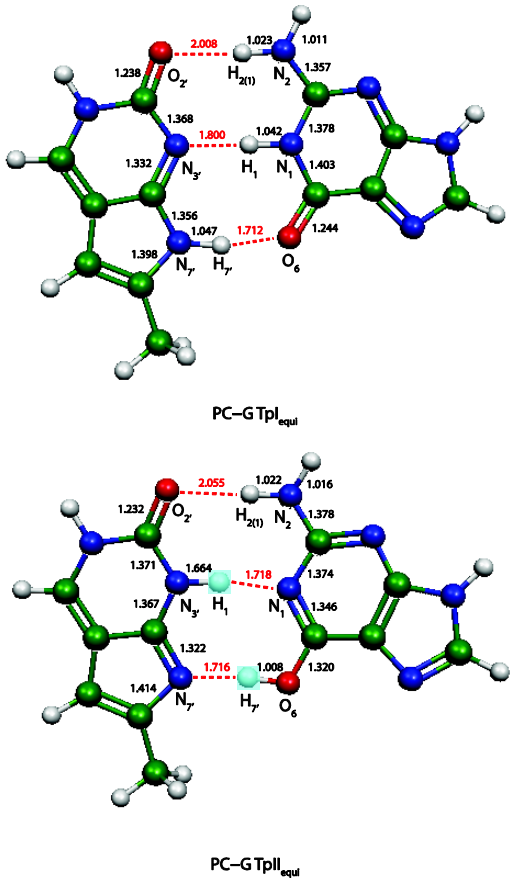

Figure 1 The ground state (S_0) equilibrium geometries of PC–G TpI_{equi} and PC–G $TpII_{equi}$ computed at MP2/cc-pVDZ level. The hydrogen bonds between PC and G, indicated by a dashed red line, are all approximately linear. The lowest energy structure is PC–G TpI_{equi}, with PC–G $TpII_{equi}$ being 0.31 eV,

7.1 kcal mol^{-1}, higher in energy. Bond distances are in Angstroms. No such structure is shown for PC–G TpIII as an optimised geometry in the ground state was not located for this tautomer pair.

Vertical Excitation Energies and Equilibrium Structures of Excited State Pyrrolocytosine-Guanine Tautomers

The vertical transition energies from PC–G TpI_{equi} to the first three excited states are shown in Table 1, along with the oscillator strength, *f*, for the transition and the assignment of the state based on the orbitals involved. The geometries of the three excited states, S_1, S_2 and S_3, were optimised successfully and are shown in Figure 2. The vertical transition energies to the ground states from the excited states in their optimised geometries are also shown in Table 1.

		From optimised S_0 geometry		**From optimised S_X geometry**	
Transition S_0 to S_x	**Assignment**	**Δ*E*/eV**	***f***	**Δ*E*/eV**	***f***
X=1	$^1\pi_{PC}{}^1\pi^*_{PC}$	4.77	0.30	4.07	0.27
X=2	$^1\pi_G{}^1\pi^*_G$	6.16	0.14	4.43	0.17
X=3	$^1\pi_{PC}{}^1\pi^*_{PC}$	6.40	0.02	6.15	0.07

Table 1 $S_0 \rightarrow S_X$ Vertical excitation energies, oscillator strengths and assignments of the three lowest singlet vertical transitions of PC–G TpI_{equi} for geometries optimised in both the S_0 and S_X states. Calculations performed at CIS/cc-pVDZ level.

A comparison of the optimised geometry of the S_1 state of PC–G TpI_{equi} with the optimised geometry of the ground state (S_0) shows an increase of up to 0.126 Å in hydrogen bond lengths in the excited state and a slight pyramidization of the amino group of guanine ($N_1C_2N_2H_{2(1)}$ dihedral angle = 7.3°, Figure 2). Changes to intramolecular bond lengths mostly affect pyrrolocytosine (Figure 2), supporting the assignment to the local excitation of the pyrrolocytosine monomer.

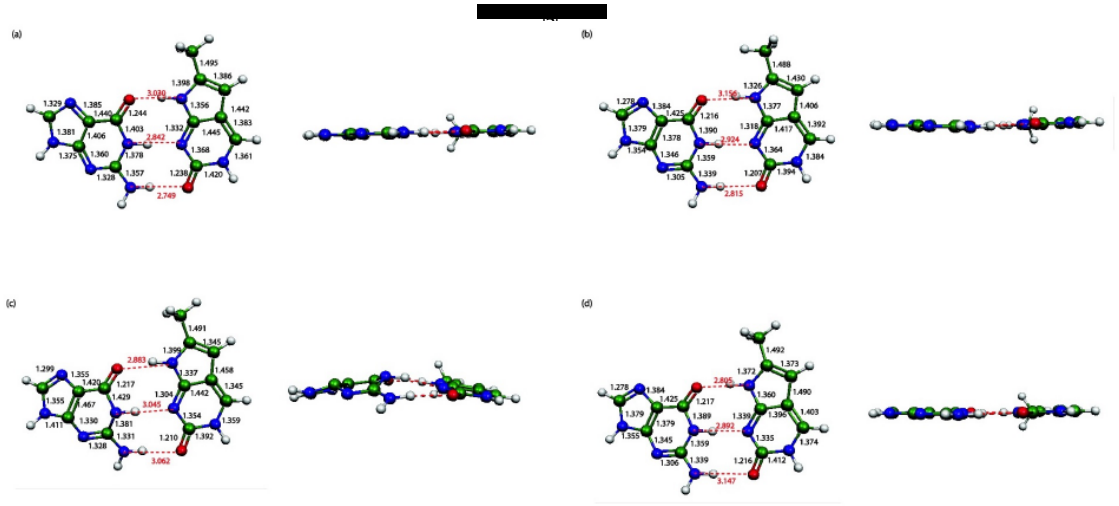

Figure 2 Optimised geometries, in plane and profile views, of the ground state (S_0) PC–G TpI_{equi} base pair (computed at MP2/cc-pVDZ level) (a), with first (S_1), second (S_2) and third (S_3) optimised electronic excited state geometries (b), (c), (d), respectively (computed at CIS/cc-pVDZ). The hydrogen bonds between PC and G, indicated by a dashed red line, are all approximately linear. Bond distances are in Angstroms.

The optimised PC–G TpI_{equi} geometry of the second (S_2) excited state has a buckled structure (Figure 2). The source of this distortion lies not in the pyramidization of the guanine amino group, but is due to an out-of-plane deformation of the ring structure of guanine caused by a twisting and shortening, from 1.360 Å in the S_0 state to 1.330 Å in the S_2 state, of the N_3C_4 bond.

The optimised geometry of the third excited state (S_3) of the PC–G TpI_{equi} base pair (Figure 2) is essentially C_s-symmetric with a slight pyramidization of the amino group of guanine ($C_{2'}C_{4'}C_6C_2$ dihedral angle of −1.3°). Hydrogen bond lengths have changed and there have been greater changes to intramolecular bond lengths affecting pyrrolocytosine, supporting the transition of $^1\pi_{PC}{}^1\pi^*_{PC}$.

For PC–G TpII, a comparison of the structure in the ground state (S_0) with the structure in the optimised first, second and third excited states (S_1, S_2, and S_3) all show an increase in hydrogen bond lengths (Figure 3). Changes to intramolecular bond lengths for the S_1 optimised PC–G $TpII_{equi}$ structure mostly affect pyrrolocytosine, which is consistent with the local excitation of the pyrrolocytosine monomer (Table 2), again there is slight pyramidization of the amino group of guanine ($N_1C_2N_2H_{2(1)}$ dihedral angle = −16.4°).

		From optimised S_0 geometry		**From optimised S_X geometry**	
Transition S_0 to S_x	**Assignment**	**ΔE/eV**	***f***	**ΔE/eV**	***f***
X=1	$^1\pi_{PC}{}^1\pi^*_{PC}$	4.50	0.19	3.85	0.11
X=2	$^1\pi_{PC}{}^1\pi^*_{PC}$	5.94	0.34	5.70	0.36
X=3	$^1\pi_G{}^1\pi^*_G$	6.13	0.28	5.89	0.44

Table 2 $S_0 \rightarrow S_X$ Vertical excitation energies, oscillator strengths and assignments of the three lowest singlet vertical transitions of PC–G $TpII_{equi}$ for geometries optimised in both the S_0 and S_X states. Calculations performed at CIS/cc-pVDZ level.

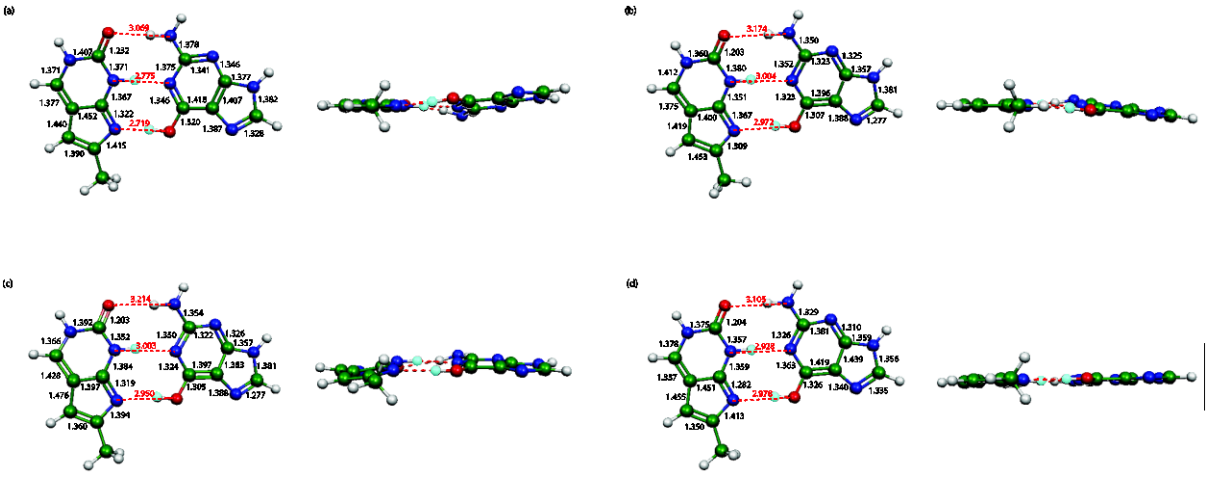

Figure 3 Optimised geometries, in plane and profile views, of the ground state PC–G $TpII_{equi}$ base pair (computed at MP2/cc-pVDZ level) (a), with first (S_1), second (S_2) and third (S_3) optimized electronic

excited state geometries (b), (c), (d), respectively (computed at CIS/cc-pVDZ). A dashed red line indicates the hydrogen bonds between PC and G. Bond distances are in Angstroms.

The S_2 optimised structure of PC–G TpII$_{equi}$ is interesting, as it is an example of significant distortion of pyrrolocytosine due to twisting of the $N_{1'}C_{6'}$ bond and the $H_{1'}N_{1'}C_{6'}H_{6'}$ dihedral angle is −15.9°, as shown in Figure 4. Perun *et al.* have observed that an out-of-plane deformation of a ring structure, such as is observed with PC–G TpII$_{equi}$ in the second (S_2) excited state, is associated with nearby conical intersections and thus potentially fast, non-radiative routes back to the ground state.[48,49] The optimised geometry of the third excited state (S_3) of PC–G TpII$_{equi}$ is C_s-symmetric (Figure 3), with the greatest changes to the intramolecular bond lengths being for guanine, consistent with local excitation of that base (Table 2).

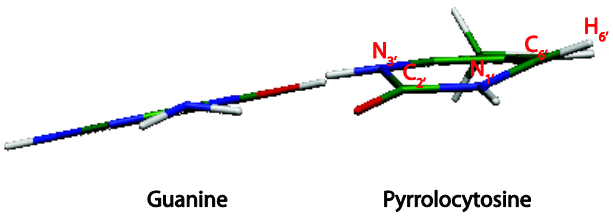

Figure 4 Optimised geometry of the S_2 excited state of the PC–G TpII$_{equi}$ structure, showing the distortion caused by twisting of the $N_{1'}C_{6'}$ bond. The $H_{1'}N_{1'}C_{6'}H_{6'}$ dihedral angle is −15.9°. Such twisting may be associated with nearby conical intersections and thus provide a fast, non-radiative, route back to the ground electronic state.

The PC-G TpIII structure, which could not be successfully optimised in the ground electronic state, was successfully optimised in the three lowest lying electronically excited states: Table 3 shows the energies of the optimised geometries whilst the structures, which are all C_s-symmetric, are shown in Figure 5.

From optimised S_X geometry			
Transition	**Assignment**	**Δ*E*/eV**	***f***
S_0 to S_x			
X=1	$^1\pi_{PC}{}^1\pi^*_{PC}$	4.72	0.10
X=2	$^1\pi_G{}^1\pi^*_G$	6.18	0.24
X=3	$^1\pi_{PC}{}^1\pi^*_{PC}$	6.61	0.33

Table 3 Vertical transition energies, oscillator strengths and assignment of the three lowest transitions between the ground electronic state and the geometry optimised excited states of the PC–G $TpIII_{equi}$ base pair. Calculations performed at CIS/cc-pVDZ level. Note excitation energies from the optimised ground state are not given as no optimised ground state structure was located.

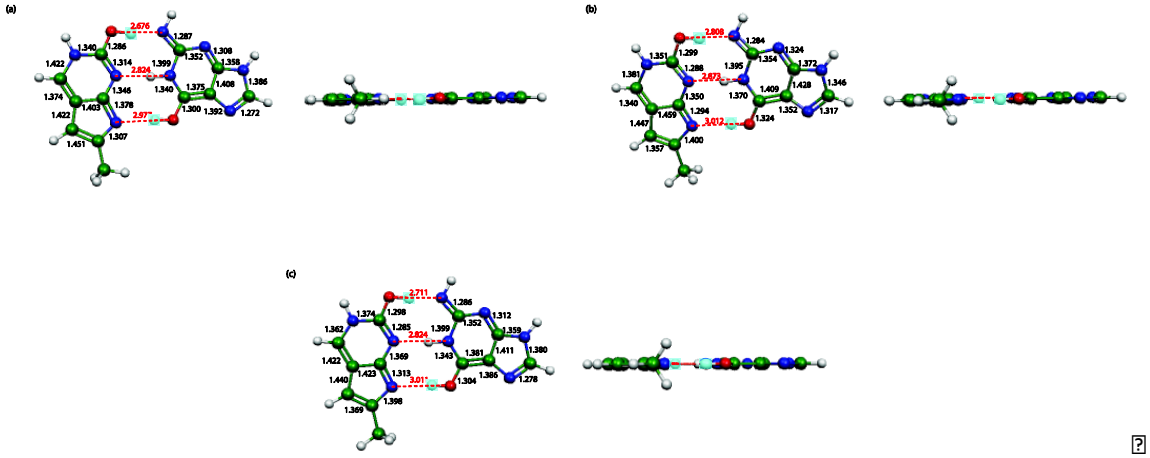

Figure 5 Optimised geometries, in plane and profile views, of the first (S_1), second (S_2) and third (S_3) electronic excited state of PC–G $TpIII_{equi}$, (a), (b) and (c), respectively (computed at CIS/cc-pVDZ). A dashed red line indicates the hydrogen bonds between PC and G. Bond distances are in Angstroms. No optimised structure for PC–G TpIII in its ground electronic state was located.

Pyrrolocytosine-Guanine Proton Transfer Potential Energy Curves in the electronic ground state

Potential energy curves for the transfer of a proton between the bases were constructed by performing a geometry optimisation whilst freezing the relevant N–H bond. As the N–H bond was frozen at longer and longer distances a proton (or potentially a hydrogen) from the other base migrated in the opposite direction, hence tautomer base pairs were formed. The general form of the potential energy curves consist of increasing energy as the frozen bond length is increased, leading to a local energy maximum ($LEnergy_{max}$), followed by a local energy minimum ($LEnergy_{min}$) when the two bases have essentially swapped protons (or hydrogens) and an alternative tautomer base pair has formed. From examination of Figure 6, which shows the potential energy curves for each of the three ground state proton transfers from PC–G TpI_{equi}, it can be seen that the $(H)N_1$ and $N_{7'}(H)$ potential energy curves have very similar profiles, which is to be expected as the result in both

cases is that the same two protons ((H)N_1 and $N_{7'}$(H)) have been exchanged between pyrrolocytosine and guanine. There is a slight difference (ΔE = ±0.04 eV or ± 0.9 kcal mol^{-1}) in the barrier heights ($LEnergy_{max}$) between these two potential energy curves. The $LEnergy_{min}$ structure formed in both cases could be optimised without any imposed geometry constraint to form PC–G $TpII_{equi}$.

The dipole moment of PC–G $TpII_{equi}$ (μ = 3.4 D) is a little higher than that of PC–G TpI_{equi} (μ = 2.4 D). Examination of the changes in dipole moments for the formation of PC–G $TpII_{equi}$ from PC–G TpI_{equi} (shown in Figure 7) reveals that the changes are quite different depending upon which proton is initially migrated. Initial migration of the H_1 proton of guanine initially increases the dipole moment between guanine and pyrrolocytosine. At the $LDipole_{max}$ structure (blue curve in Figure 7) the dipole moment is 7.0 D. The dipole moment is partially reduced by migration of a second proton ($H_{7'}$) from pyrrolocytosine to guanine. Initial migration of $H_{7'}$ from pyrrolocytosine to guanine however initially decreases the dipole moment as positive charge is being transferred from pyrrolocytosine to guanine, however the migration of the second proton (H_1) from guanine to pyrrolocytosine increases the dipole moment again.

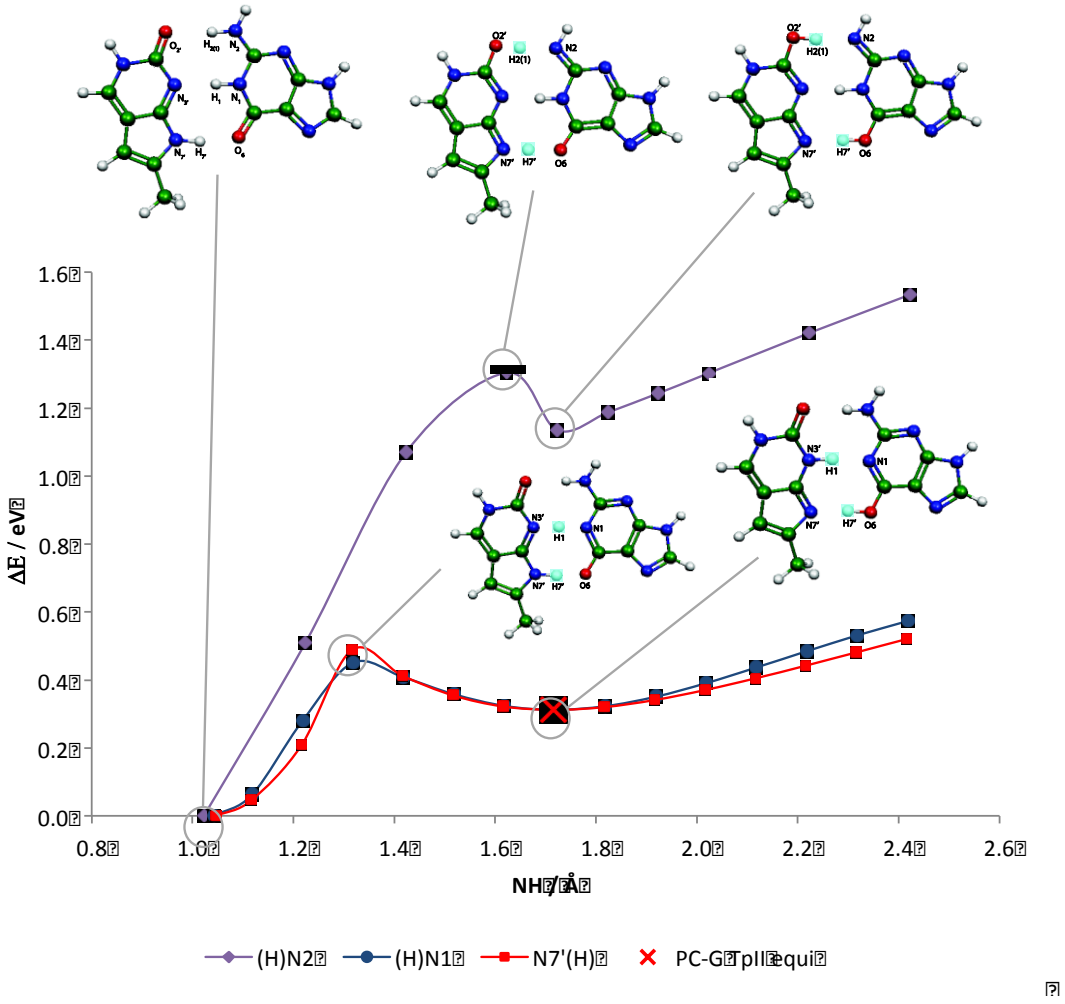

Figure 6 Change in energy of the optimised ground state (S_0) geometry as a function of H–N distance for the proton transfer processes from the PC–G TpI_{equi} structure. The top row of structures and violet line refer to moving the $O_{2'}$–(H)N_2 proton, showing the initial PC–G TpI_{equi} structure, a local energy maximum ($LEnergy_{max}$) structure at (H)N_2 at 1.623 Å and a local energy minimum ($LEnergy_{min}$) structure at (H)N_2 1.723 Å and a $O_{2'}$(H) distance of 1.033 Å. Unrestricted geometry optimisation of the $LEnergy_{min}$ (H)N_2–N_7(H) double proton transfer structure was not successful in that a structure for PC–G $TpIII_{equi}$ was not located, rather the system reverted to PC–G TpI_{equi}. The lower pair of structures refer to moving the $N_{3'}$–(H)N_1 (blue line) and $N_{7'}$(H)–O_6 (red line) protons: the left figure showing a local energy maximum ($LEnergy_{max}$) at $N_{7'}$(H) = 1.316 Å and the right figure showing the

structure of PC–G $TpII_{equi}$ (✖ on potential energy curve) produced by unrestricted geometry optimisation.

As the $(H)N_2$ proton migrates from the amino group of guanine to pyrrolocytosine, a local energy maximum ($LEnergy_{max}$) is reached at a $(H)N_2$ bond length of 1.623 Å (Figure 6) and forms a barrier ΔE = 1.30 eV (30.0 kcal mol^{-1}) above the PC–G TpI_{equi} ground state energy. The migration of a second proton $H_{7'}$, from pyrrolocytosine to guanine, leads to the formation of a local energy minimum ($LEnergy_{min}$) structure at $(H)N_2$ = 1.723 Å, but the reduction in energy is only slight and this $LEnergy_{min}$ structure reverted to PC–G TpI_{equi} upon attempts to optimise it. During transfer of the $(H)N_2$ proton from guanine to pyrrolocytosine the magnitude of the maximum dipole moment ($LDipole_{max}$), shown in Figure 8, is higher by at least 7.0 D than was found for the $(H)N_1$ and $N_{7'}(H)$ proton transfers, indicating increased charge separation as the $(H)N_2$ proton is transferred from one moiety to the other.

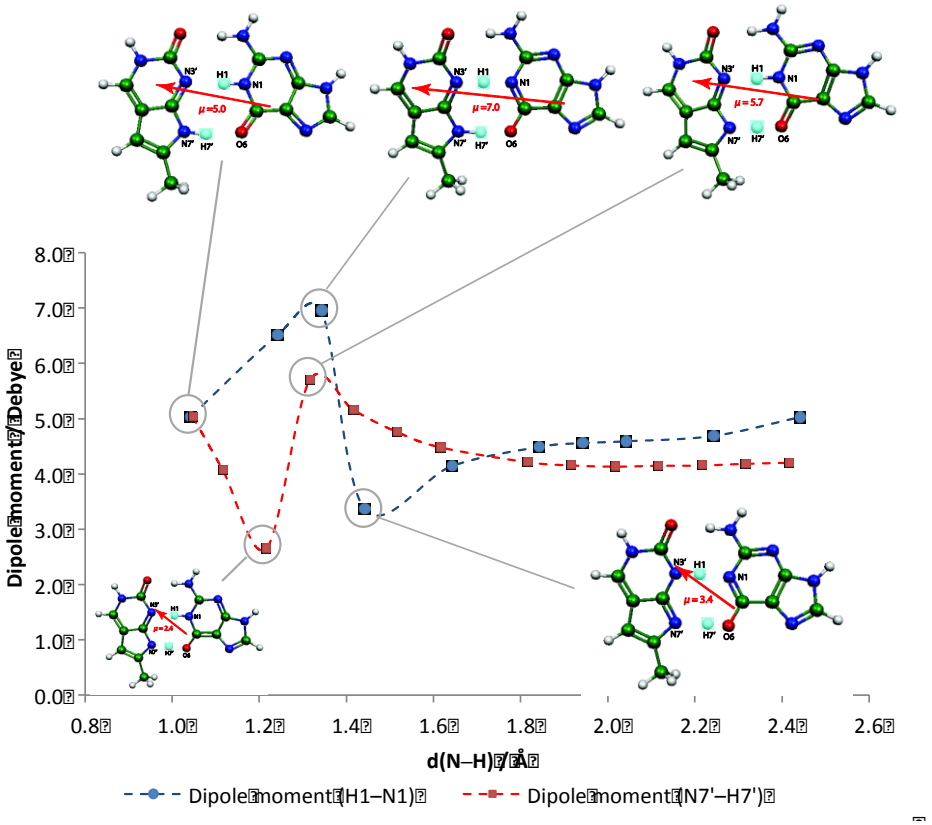

Figure 7 Dipole moment as a function of N–H distance for the (H)N_1 and $N_{7'}$(H) proton transfers from the ground state (S_0) optimised PC–G TpI_{equi} structure. Showing (top row of figures left to right) PC–G TpI_{equi} structure, $LDipole_{max}$ for (H)N_1 proton transfer and $LDipole_{max}$ for $N_{7'}$(H) proton transfer. Left inset figure is $LDipole_{min}$ for $N_{7'}$(H) proton transfer and right inset figure is $LDipole_{min}$ for N_1(H) proton transfer.

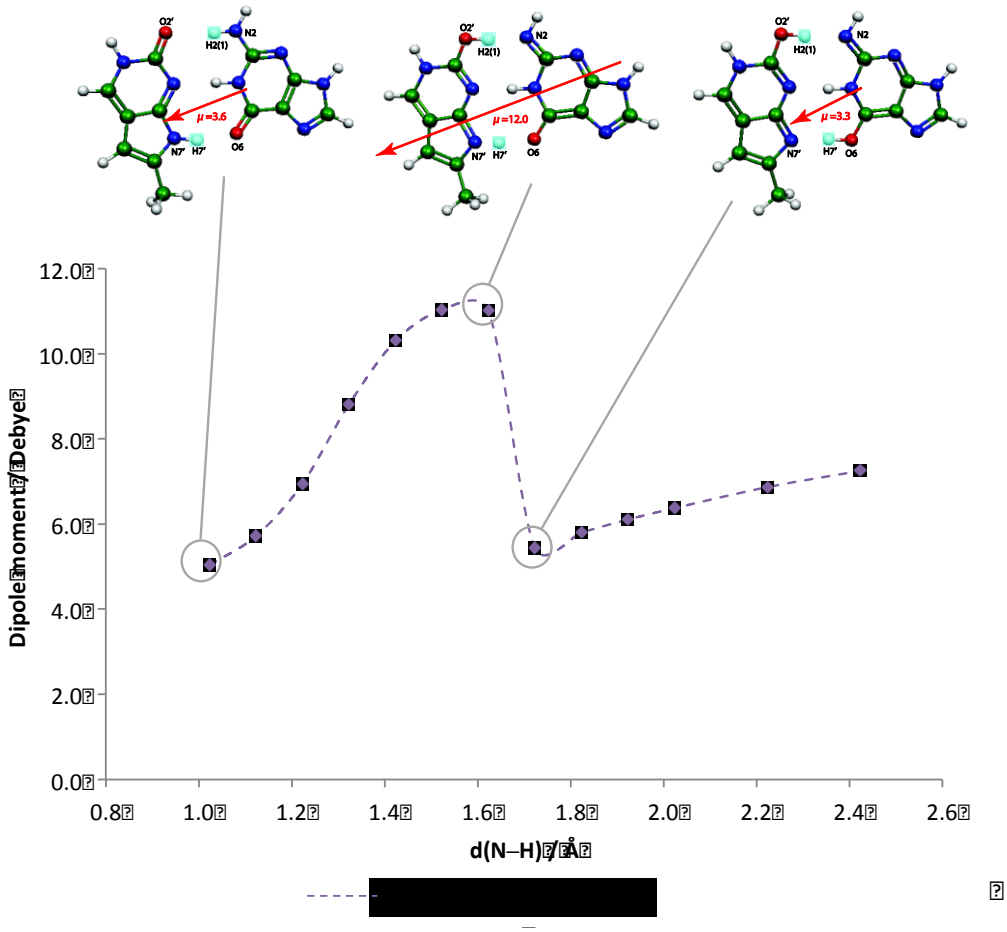

Figure 8 Change in dipole moment of the optimised ground state (S_0) geometry as a function of H_2 to N_2 distance for the proton transfer process $O_{2'}$–(H)N_2 from PC–G TpI_{equi}. Showing the TpI_{equi} structure of PC–G, a local maximum in the dipole moment of (H)N_2 at 1.623 Å and a local minimum in the dipole moment at (H)N_2 1.723 Å and a $O_{2'}$(H) distance of 1.033 Å.

Pyrrolocytosine-Guanine Proton Transfer Potential Energy Curves in electronically excited states

Transfer of protons to form alternative tautomer pairs in the first electronically excited state was explored in a similar manner to the ground state, by performing a, in this case excited state,

geometry optimisation whilst freezing the relevant N–H bonds at increasing longer lengths. The potential energy (Figure 9) and dipole moment curves (Figure 10) for the PC–G proton transfers in the first excited state have a very similar profile to those of the ground state (S_0) (Figures 6,7 and 8), the key difference being that although in the ground electronic state it was not possible to optimise PC–G $TpIII_{equi}$, this was possible in the first excited state (S_1).

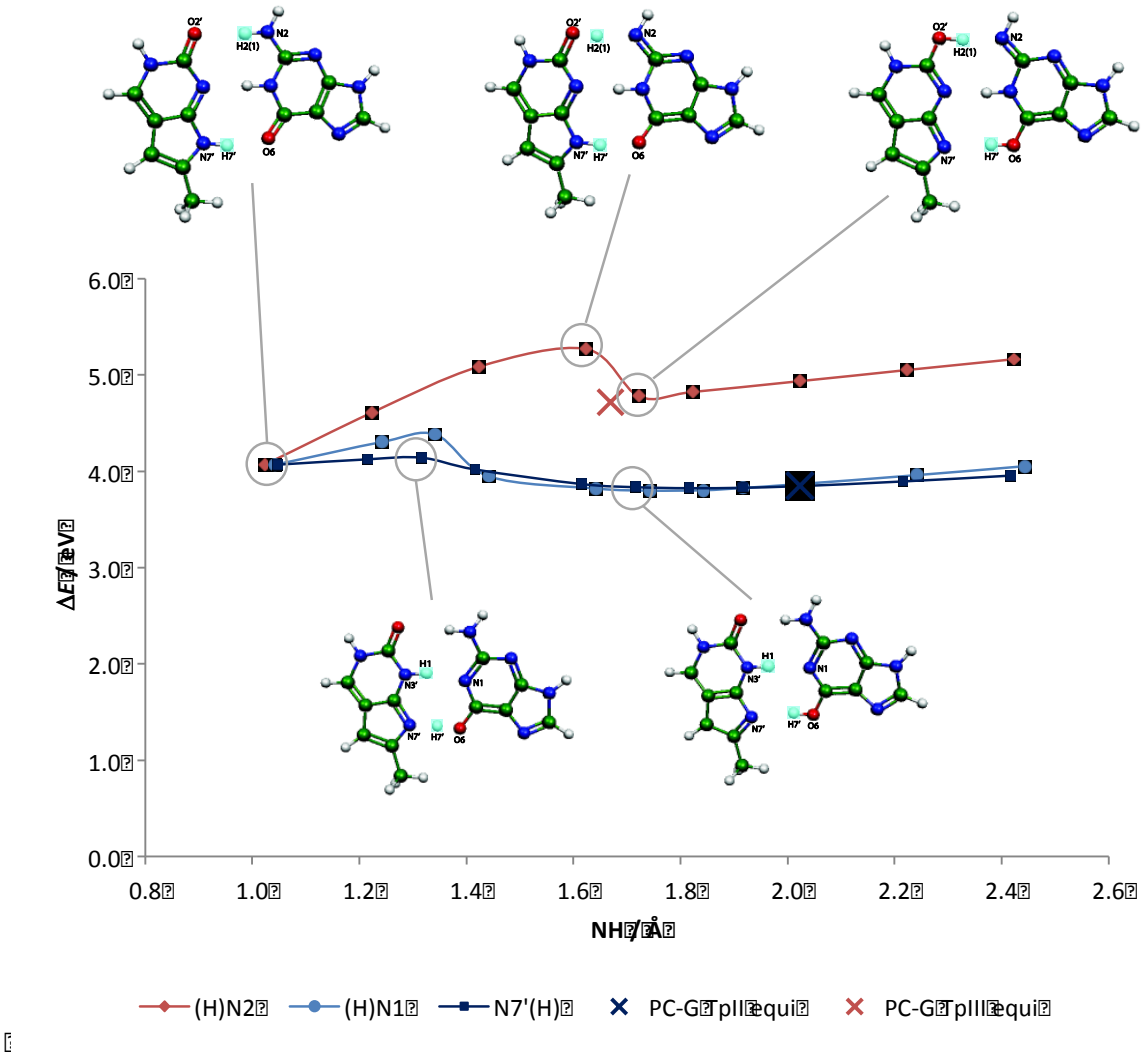

Figure 9 Potential energy as a function of N–H distance for the (H)N_2, (H)N_1, $N_{7'}$(H) proton transfers from the S_1 PC−G TpI_{equi} structure, and the energies of the PC–G $TpII_{equi}$ (✖) & PC–G $TpIII_{equi}$ (✖) optimised S_1 geometries. Calculations were performed at the CIS/cc-pVDZ level. In the S_1 state the PC–G $TpII_{equi}$ structure is lower in energy than the PC–G TpI_{equi} structure.

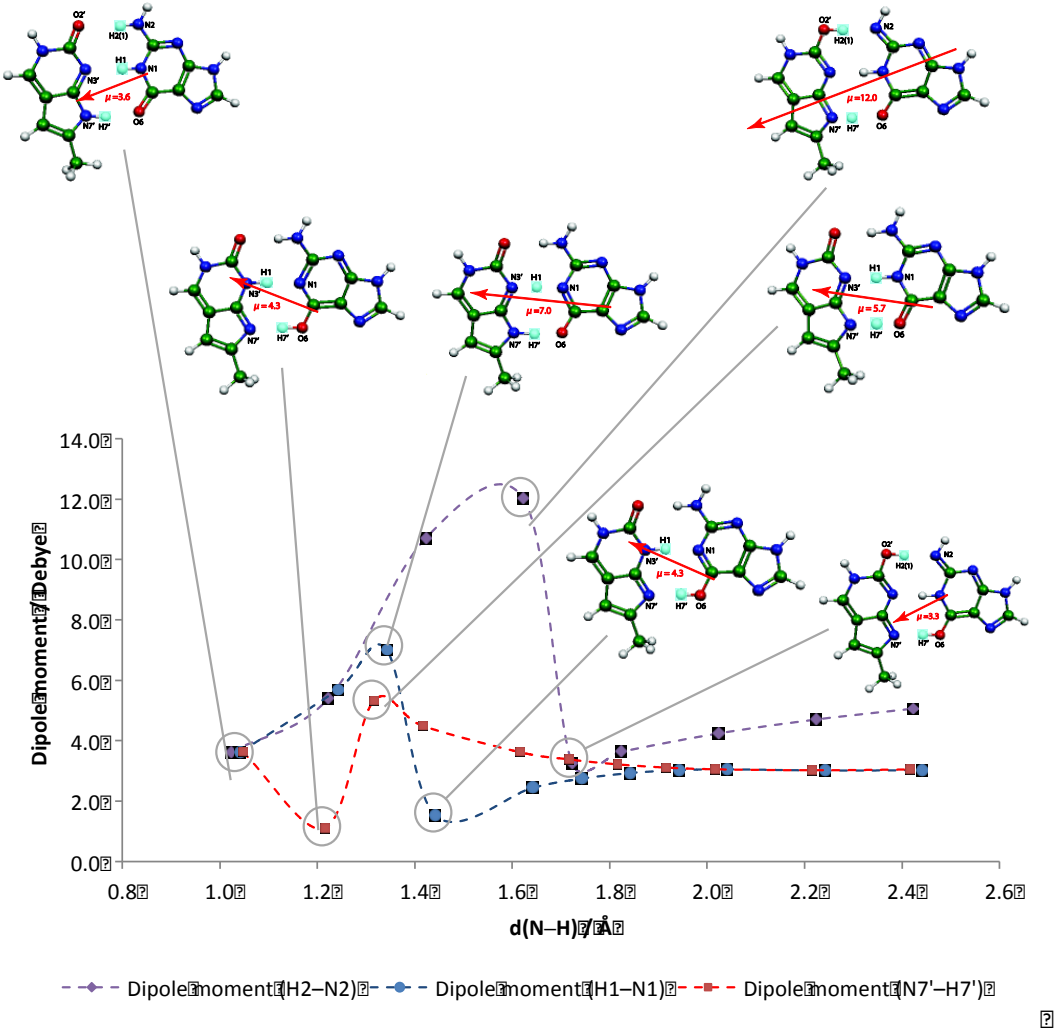

Figure 10 Dipole moment as a function of N–H distance for the (H)N_2, (H)N_1 and $N_{7'}$(H) proton transfers from the PC–G TpI_{equi} structure in the S_1 optimised geometries. Showing (top row of figures left to right) PC–G TpI_{equi} and $LDipole_{max}$ for (H)N_2 proton transfer; (middle row of figures left to right) $LDipole_{min}$ for $N_{7'}$(H), $LDipole_{max}$ for (H)N_1 and $LDipole_{max}$ for $N_{7'}$(H) proton transfers; (bottom row of figures left to right) $LDipole_{min}$ for (H)N_1 and (H)N_2 for $LDipole_{min}$ proton transfers.

Possible conversion pathways between PC–G TpI , PC–G TpII and PC–G TpIII

PC–G TpI is the more stable structure in the ground electronic state, whilst PC–G TpII is more stable in the first excited state. In the ground state only a very small fraction of PC–G would be expected in PC–G TpII as this structure is over 7 kcal mol^{-1} higher in energy than PC–G TpI. Excitation of PC–G TpI to S_1 requires 4.77 eV (Table 1), which could lose 0.70 eV as it undergoes vibrational relaxation to the optimised S_1 structure of PC–G TpI, which is 4.07 eV above the ground state. However, as the energy of optimised geometry of PC–G TpII in the first excited state, 3.85 eV, is lower by 0.22 eV (5 kcal mol^{-1}), than the initially formed excited state PC–G TpI, double proton transfer is possible to yield PC–G TpII in the excited state. Note that 4.77 eV is higher in energy than the barrier at about 1.3 Å shown on Figure 9. Once formed in the excited state PC–G $TpII_{equi}$ would provide an alternative route back to the ground electronic state, either via fluorescence back to the ground electronic state of PC–G TpII or via some other route. Once formed, ground state PC–G TpII could convert back to PC–G TpI by crossing the local energy maximum barrier, 3.205 kcal $mol^{-1,}$ at 1.318 Å shown on Figure 6. Excitation of PC–G TpI to the first excited state does not provide sufficient energy to cross the barrier located at about 1.6 Å required to form PC–G TpIII in the first excited state by double proton transfer.

Two possible tautomer pairs for 2-aminopurine-thymine (2AP–T) are shown in Scheme 1. The MP2 optimised geometry of the 2AP–T TpI_{equi} base pair, equivalent to the lowest energy tautomer pair for the natural base pair A-T, was the only tautomer pair for which a minimum energy structure was found in the ground electronic state. The optimised structure is buckled (Figure 11), owing to pyramidization of the amino group of 2-aminopurine (2AP) with a $N_{1'}C_{2'}N_{2'}H_{2'(1)}$ dihedral angle of 22.3°. This pyramidization of the amino group of 2-aminopurine is greater than that seen in the equivalent structure for A-T, where the $H_{2'}$-N_6-C_6-$N_{1'}$ dihedral angle is 12.5° when A-T is optimised at the same level. The thymine in the 2AP–T and A-T base pairs has a flat ring structure. The two hydrogen bonds between 2AP and T are approximately linear, as expected (within 5° of 180°). The equivalent two hydrogen bonds lengths and angles in the A-T base pair optimised at the same level are within 0.1 Å and 2° of those in 2AP-T.

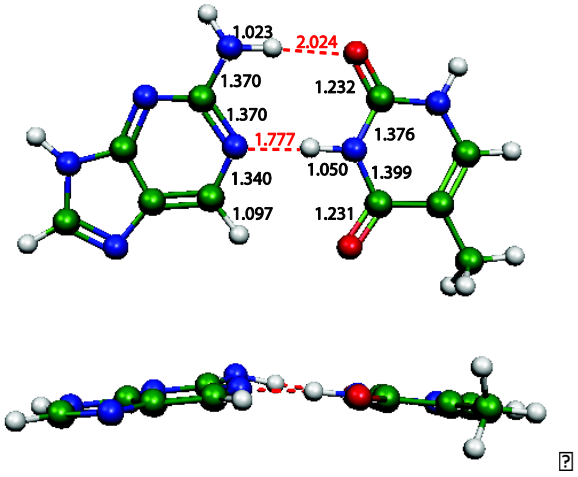

Figure 11 The ground state (S_0) equilibrium geometry of 2AP–T TpI_{equi} at MP2/cc-pVDZ level. Bond lengths are given in Angstroms. No such structure is shown for 2AP–T TpII as an optimised geometry in the ground state was not located for this tautomer pair.

Vertical Excitation Energies and Equilibrium Structures of Excited State 2-Aminopurine-Thymine Tautomers

The vertical transition energies from 2AP–T TpI_{equi} to the first three excited states are shown in Table 4, along with the oscillator strength, *f*, for the transition and the assignment of the state based on the orbitals involved. The geometries of the three excited states, S_1, S_2 and S_3, were optimised successfully and are shown in Figure 12. The vertical transition energies from the optimized excited states to the ground states are also shown in Table 4. The hydrogen bond lengths of the 2AP–T TpI_{equi} base pair in the ground state (S_0), first (S_1), second (S_2) and third (S_3) excited states are shown in Figure 12.

Transition S_0 **to** S_x	**Assignment**	**From optimised S_0 geometry** Δ*E*/eV	*f*	**From optimised S_x geometry** Δ*E*/eV	*f*
X=1	$^1\pi_{2AP}{}^1\pi^*_{2AP}$	5.57	0.38	5.12	0.41
X=2	$^1n_T{}^1\pi^*_T$	6.30	0.00	4.85	0.00
X=3	$^1\pi_T{}^1\pi^*_T$	6.42	0.30	5.32	0.16

Table 4 $S_0 \rightarrow S_X$ Vertical excitation energies, oscillator strengths and assignments of the three lowest singlet vertical transitions of the optimised geometries of the 2AP–T TpI_{equi} for geometries optimised in both the S_0 and S_X states. Calculations performed at CIS/cc-pVDZ level.

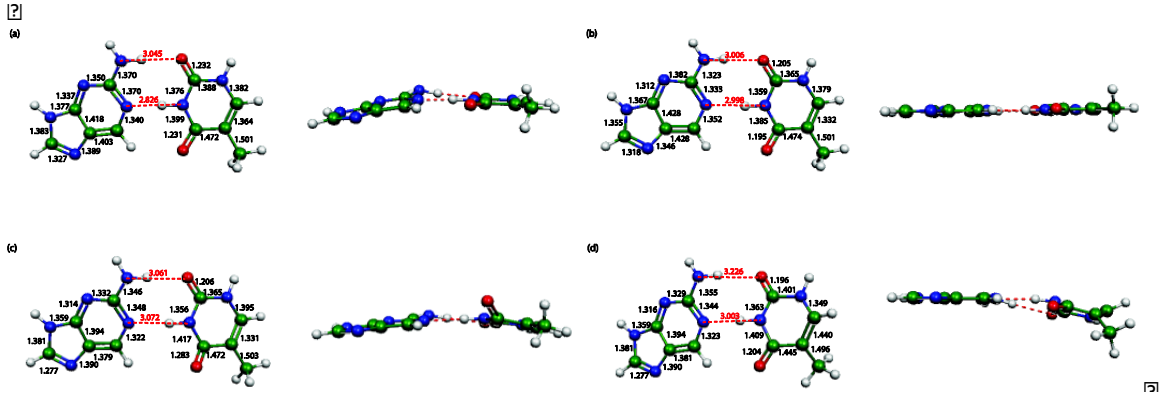

Figure 12 Optimised geometries, in plane and profile views, of the ground state (S_0) 2AP–T TpI_{equi} base pair (computed at MP2/cc-pVDZ level), (a), and the first (S_1), second (S_2) and third (S_3) electronic excited state geometries (b), (c), (d), respectively (computed at CIS/cc-pVDZ). A dashed red line indicates the hydrogen bonds between 2AP and T.

Bond distances are in Angstroms.

The third transition (S_3) of 2AP–T TpI_{equi} is interesting in terms of changes to the geometry of the base pair, shown by twisting of the C_5C_6 double bond of thymine which has a $H_6C_6C_5C_7$ dihedral angle of −61.2°. This distortion may indicate the presence of a nearby conical intersection present in thymine, as described by Perun *et al.*,[49] which features out-of-plane distorted geometries of the six-membered heteroaromatic ring. Whereby, the H_6 atom and methyl group are twisted out of the plane of the ring (Figure 12) and the C_5C_6 bond increases in length by 0.076 Å. These geometrical changes in thymine are consistent with $^1LE(\pi_T\pi^*_T)$ excitation.

The 2AP–T TpII structure can be formed by exchanging a proton from the $(H)N_3$ of thymine to 2-aminopurine and the $N_{2'}(H)$ of 2-aminopurine to thymine. Although an optimised structure for 2AP–T TpII could not be found in the ground electronic state, this tautomeric pair could be successfully optimised in the first electronically excited state, although it was higher in energy than the first

excited state of the 2AP–T TpI$_{equi}$ structure. The S_1 structure of 2AP–T TpII$_{equi}$ has a $N_{2'}$(H) bond length of 1.812 Å with a ΔE = 0.40 eV (9.2 kcal mol^{-1}) above the S_1 optimised 2AP–T TpI$_{equi}$ structure. Table 5 shows the vertical transition energies from the optimised geometries of the three lowest lying excited states of 2AP–T TpII$_{equi}$. Vertical transition energies from the optimised ground state (S_0) are not shown since 2AP–T TpII$_{equi}$ could not be optimised in its ground state (S_0) geometry.

From optimised S_X geometry			
Transition S_0 **to** S_x	**Assignment**	**Δ*E*/eV**	***f***
X=1	$^1\pi_{2AP}{}^1\pi^*_{2AP}$	5.53	0.24
X=2	$^1\pi_T{}^1\pi^*_T$	6.62	0.23
X=3	$^1 n_T{}^1\pi^*_T$	6.66	0.00

Table 5 Vertical transition energies, oscillator strengths, *f*, and assignment of the three lowest transitions of the optimised geometries of the 2AP–T $TpII_{equi}$ 2-aminopurine-thymine base pair. Calculations performed at CIS/cc-pVDZ level. Note excitation energies from the optimised ground state are not given as no optimised ground state structure was located.

The geometries of the optimised S_1, S_2 and S_3 structures of 2AP–T $TpII_{equi}$ are shown in Figure 13. The geometry of 2AP–T $TpII_{equi}$ in the first excited state (S_1) is flat with a $C_{6'}C_{2'}C_2C_4$ dihedral angle of 0.0°, whereas the optimised geometry of the second excited state (S_2) has a puckered structure, due to twisting of the N_1C_6 bond of thymine, with a $H_1N_1C_6H_6$ dihedral angle of 17.4°. The S_3 optimised structure of 2AP–T $TpII_{equi}$ is also distorted, here by a twisting of the C_5C_6 bond of thymine, with a $C_7C_5C_6H_6$ dihedral angle of 37.5°.

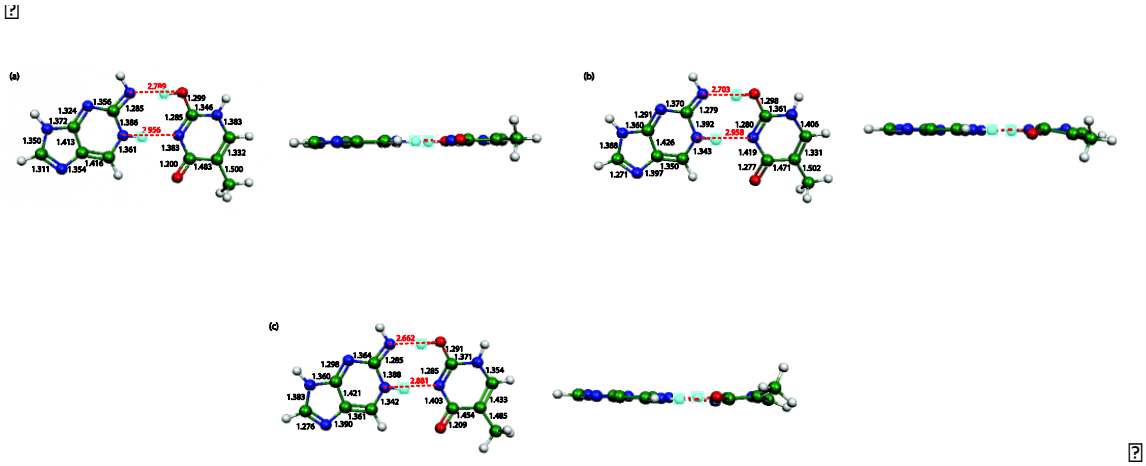

Figure 13 Optimised geometries, in plane and profile views, of the 2-aminopurine-thymine base pair with first (S_1), second (S_2) and third (S_3) electronic excited state geometries of 2AP–T $TpII_{equi}$ (a), (b) and (c), respectively (computed at CIS/cc-pVDZ). A dashed red line indicates the hydrogen bonds between 2AP and T. Bond distances are in Angstroms.

2-Aminopurine-Thymine Proton transfer Potential Energy Curves in the electronic ground state

Examination of the potential energy curve (Figure 14) for the migration of the $N_{2'}(H)$ proton from 2-aminopurine to thymine, in the ground electronic state, shows that there are no clearly defined $LEnergy_{max}$ or $LEnergy_{min}$ structures observed as was previously seen for the potential energy curves of proton transfer in the pyrrolocytosine-guanine base pair, and, as has been noted previously, no optimised structure was found for 2AP–T TpII. Any attempt to optimise the structure at the $LDipole_{min}$ without imposed geometry constraints produces the 2AP–T TpI_{equi} structure.

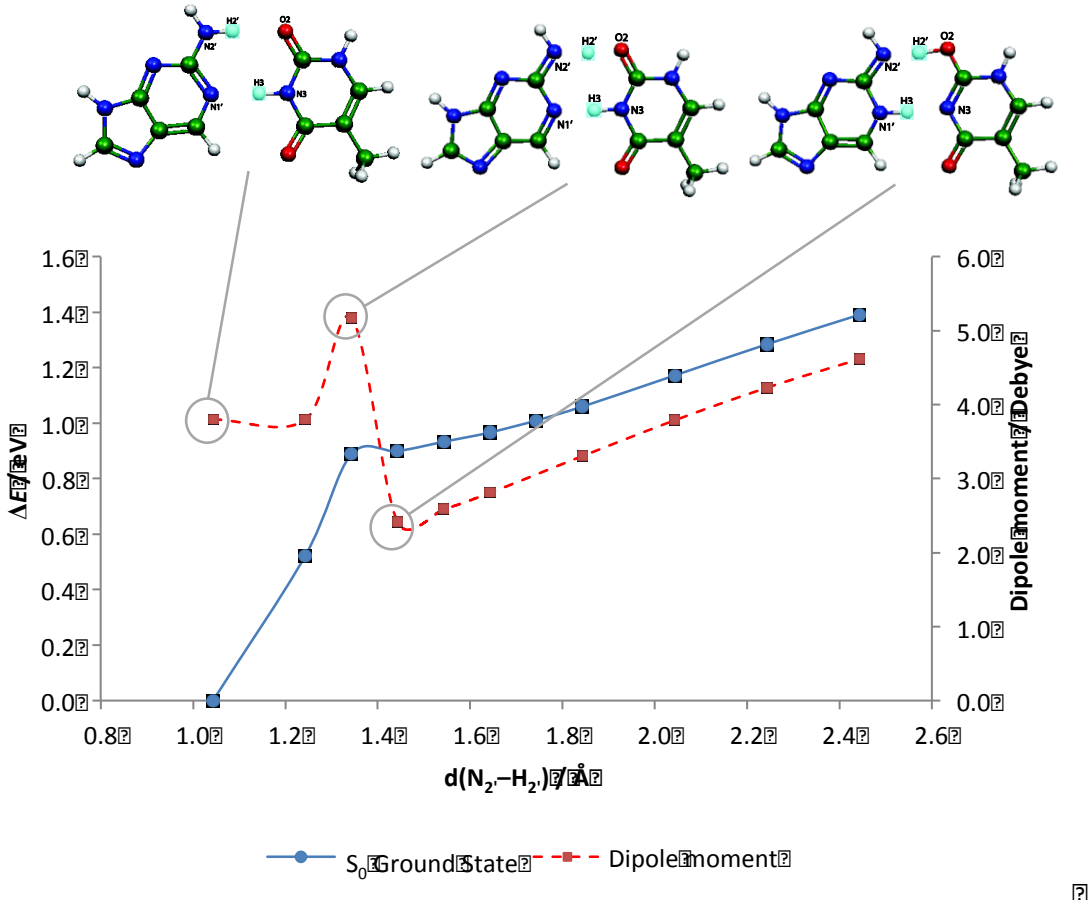

Figure 14 Change in energy of the optimised ground state (S_0) geometry as a function of $N_{2'}$ to $H_{2'}$ distance of the gas phase 2AP–T TpI_{equi} base pair for the proton transfer process $N_{2'}(H)$–O_2. Showing the 2AP–T TpI_{equi} structure, a local dipole maximum ($LDipole_{max}$) of $N_{2'}(H)$ at 1.343 Å and a local dipole minimum ($LDipole_{min}$) at $N_{2'}(H)$ = 1.443 Å and a $(H)O_2$ distance of 1.121 Å. No $LEnergy_{min}$ structure for 2AP–T TpII was located and unrestricted geometry optimisation of initial geometries for 2AP–T TpII, performed at MP2/cc-pVDZ level, did not locate a minimum energy structure for this tautomer pair.

Migrating the proton (or hydrogen) from $(H)N_3$ first leads to a slightly different situation (Figure 15). A local energy maximum structure was located at a relatively large $(H)N_3$ bond distance, $(H)N_3$ = 1.950 Å, with an energy barrier of ΔE = 0.96 eV (22.1 kcal mol^{-1}) above the 2AP–T TpI_{equi} structure.

However, as the migration of the (H)N_3 proton proceeds the alignment of hydrogen bond donors and acceptors adjusts and the previously migrated (H)N_3 proton is now attached to the O_4 atom of thymine and is hydrogen bonded to $N_{1'}$ of 2-aminopurine. This geometrical distortion is also accompanied by a rapid decrease in energy of the potential energy curve by ΔE = 0.55 eV (12.7 kcal mol^{-1}) at the $LEnergy_{min}$ structure (Figure 15). As a consequence, it is not possible to form 2AP–T $TpII_{equi}$ by migration of the (H)N_3 proton from thymine to 2-aminopurine.

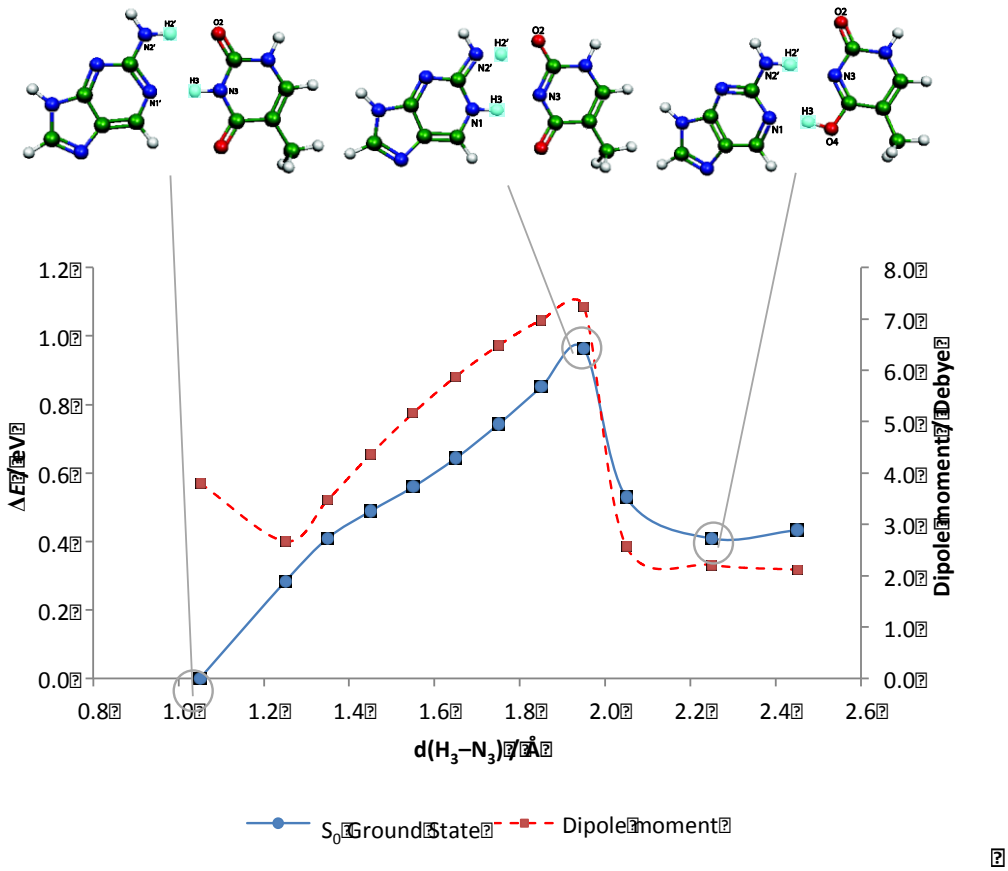

Figure 15 Change in energy of the optimised ground state (S_0) geometry as a function of H_3 to N_3 distance of the gas phase 2AP–T base pair for the proton transfer process $N_{1'}$–(H)N_3. Showing the 2AP–T TpI_{equi} structure, a local energy maximum ($LEnergy_{max}$) of $N_{2'}$(H) at 1.950 Å and finally a

rearrangement such that 2-aminopurine is in its original tautomeric form and thymine is in an alternative tautomeric form. An equilibrium structure for 2AP–T TpII could thus not be located.

2-Aminopurine-Thymine Proton Transfer Potential Energy Curves in excited electronic ground states

The potential energy curve of the optimised first excited state (S_1) starting from 2AP–T TpI_{equi} with the migration of the $N_{2'}(H)$ proton from 2-aminopurine to thymine comprises, with one exception, of $^1LE(\pi\pi^*)$ transitions on 2-aminopurine (Figure 16). There is a local energy maximum at $(H)N_2 = 1.343$ Å, that is $\Delta E = 0.66$ eV (15.2 kcal mol^{-1}) above the S_1 2AP–T TpI_{equi} structure. There is also a reduction in hydrogen bond distances between the 2AP–T base pairs at the $LEnergy_{max}$ structure (middle base pair of top row Figure 16).

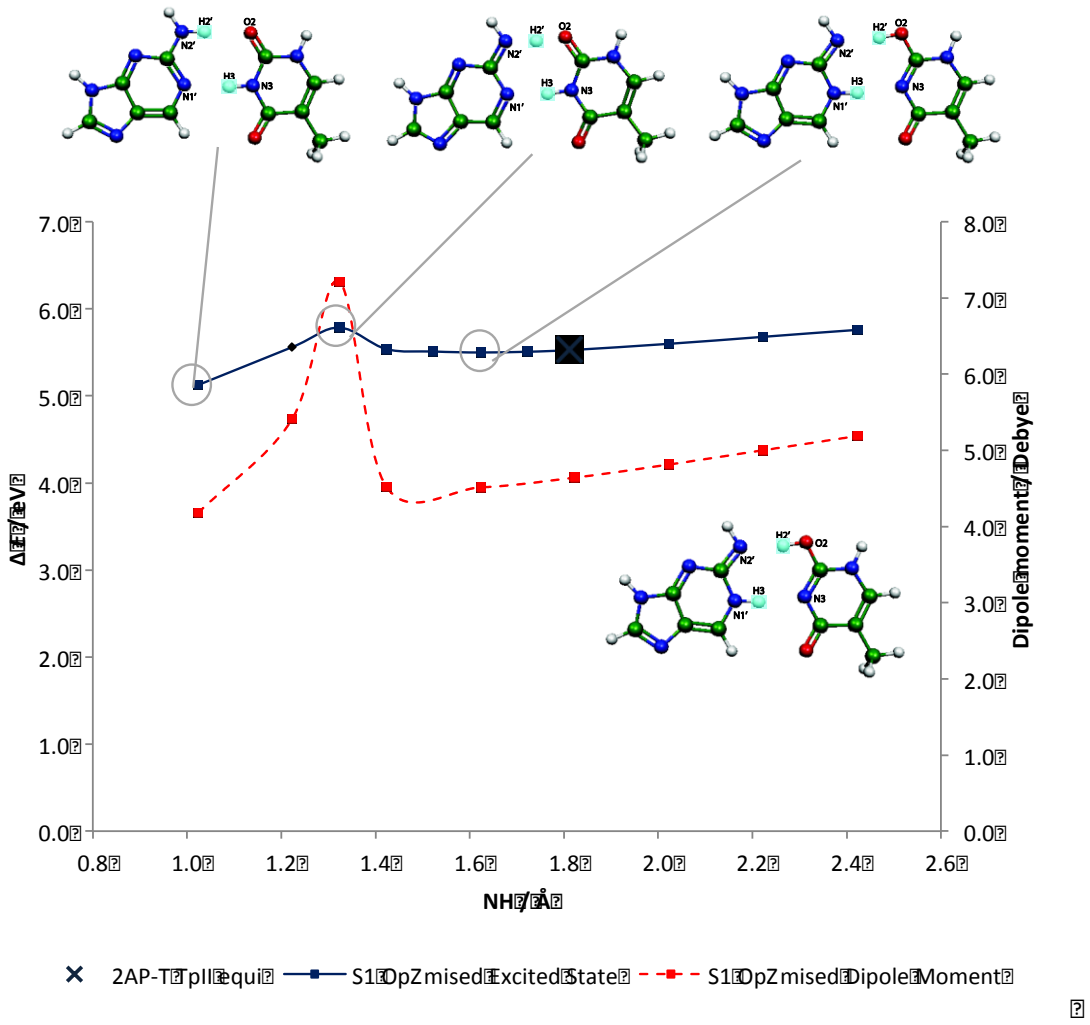

Figure 16 Change in energy and dipole moment of the gas phase optimised geometry for the first electronic excited state of the 2AP–T base pair for the proton transfer process $N_{2'}(H)$–O_2. Showing the structure of 2AP−T TpI_{equi}, the local energy maximum structure of $N_{2'}(H)$ at 1.323Å and 2AP–T $TpII_{equi}$ at $N_{2'}(H)$ = 1.812Å produced by unrestricted geometry optimisation (✕ on potential energy curve) is shown as an inset figure on the plot. The symbols ◆ represents a state with some charge transfer character, ($\pi_{2AP}\pi^*_T$).

Transfer of a second proton (H_3) from thymine to 2-aminopurine results in the formation of a $LEnergy_{min}$ structure at $(H)N_2$ = 1.623 Å (Figure 16). There is a decrease in both the energy (ΔE = 0.25 eV or 5.8 kcal mol^{-1}) and dipole moment (Δ❍ = 2.7 D) from the S_1 optimised $LEnergy_{max}$ to the S_1 optimised $LEnergy_{min}$ structures. The optimised S_1 $LEnergy_{min}$ structure is higher in energy (ΔE = 0.38 eV or 8.8 kcal mol^{-1}) than the S_1 optimised 2AP–T TpI_{equi} structure. The geometry optimised structure of 2AP–T $TpII_{equi}$ in its first electronically excited state (S_1) was found by the optimisation of the S_1 $LEnergy_{min}$ structure at CIS level without applying a geometry constraint.

The form of the potential energy curve of the S_1 optimised geometry as a function of H_3–N_3 distance (Figure 17) closely follows the shape of the S_0 ground state, with a local energy maximum found at $(H)N_3$ = 1.950 Å which is 0.69 eV (15.9 kcal mol^{-1}) above the S_1 optimised 2AP–T TpI_{equi} structure. The dipole moment of the S_1 optimised geometries form a similar curve to that of the S_0 ground state (Figure 15), reaching a local maximum (μ = 8.7 D) at $(H)N_3$ = 1.950 Å (Figure 17).

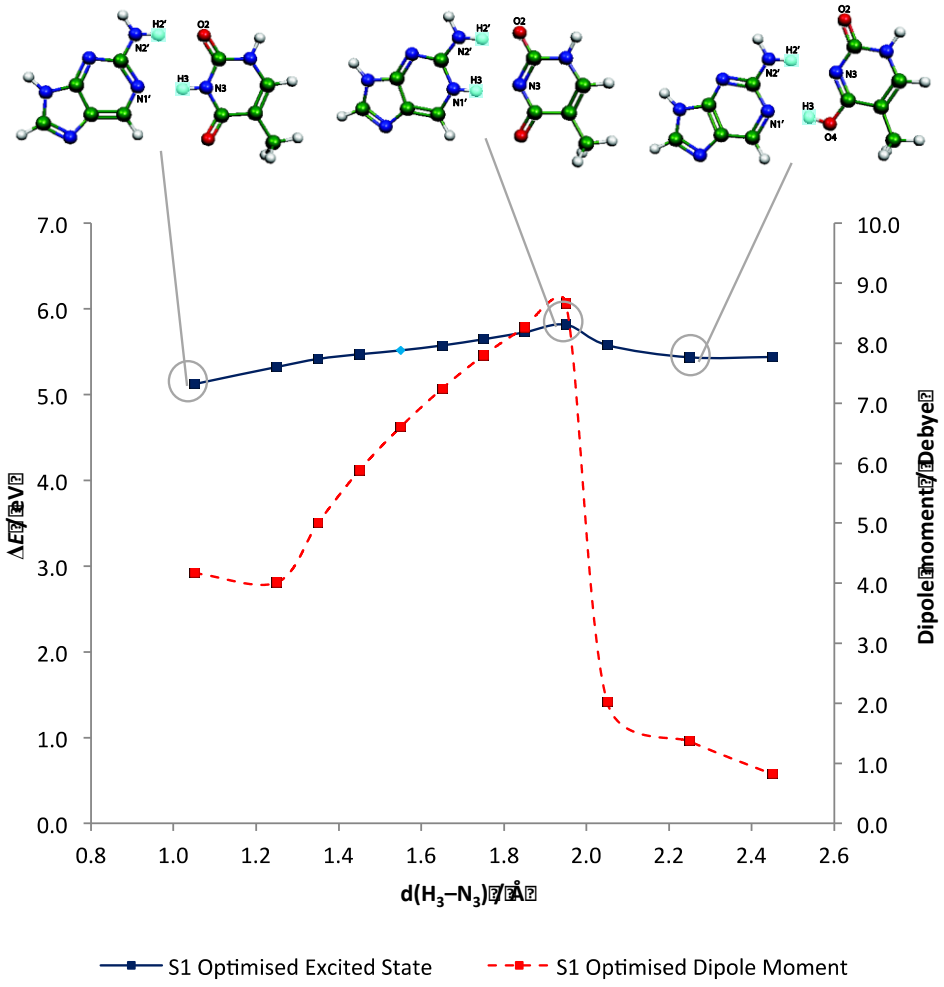

Figure 17 Change in energy and dipole moment of the optimised geometry of the gas phase for the first electronic excited state (S_1) of the 2AP–T base pair for the proton transfer process $N_{1'}$–(H)N_3. Showing the 2AP–T TpI_{equi} structure of 2AP–T and the single proton transfer structure at (H)N_3 1.950 Å. The ◆ represents a state with some charge transfer character, $\pi_{2AP}\pi^*_T$.

Possible conversion pathways between 2AP–T TpI and 2AP–T TpII

Conversion from 2AP–T TpI to 2AP–T TpII in neither the ground nor first electronically excited state is likely. In the ground state only 2AP–T TpI was found to be stable. In the first excited state, although 2AP–T TpII could be optimized to yield a minimum energy structure in this tautomeric form, the structure is less stable than 2AP–T TpI in the first excited state and there is insufficient energy in the $S_0 \rightarrow S_1$ vertical transition at the 2AP–T TpI_{equi} structure to surmount the S_1 optimised potential energy barrier at $N_{2'}(H)$ = 1.323 Å and form 2AP–T TpII in the excited state.

CONCLUSION

Three base pair tautomers of PC–G were studied. In the electronic ground state the lowest energy tautomer pair was found to be PC–G TpI_{equi}, which is analogous to the lowest energy tautomer pair of C–G. A second tautomer pair, PC–G $TpII_{equi}$ was found but was less thermodynamically stable than PC–G TpI_{equi} in the ground electronic state. A third structure, PC–G $TpIII_{equi}$, was not found to be stable in the ground electronic state. In the first electronically excited state however, PC–G $TpII_{equi}$ was found to be more stable than PC–G TpI_{equi}. It is suggested that excitation of PC–G TpI_{equi} to the first electronically excited state could lead to the formation, via double proton transfer, of electronically excited PC–G $TpII_{equi}$, which would return to the ground electronic state, forming ground state PC–G $TpII_{equi}$. Thus an excited state double proton transfer reaction could provide an alternative route for electronically excited pyrrolocytocine to return to the electronic ground state when in a base paired environment, and thus may be responsible for the different fluorescence properties of pyrrolocytosine in hydrogen bonded environments, compared to when not hydrogen bonded.

In the case of the 2-aminopurine-thymine base pair, only one tautomer 2AP–T TpI_{equi}, which is analogous to the A–T structure, was found to be stable in the ground electronic state. In the first electronically excited state a second tautomer pair structure was found to be stable, 2AP–T TpII but this structure is less stable than the 2AP–T TpI_{equi} in the first excited state, and excitation of 2AP–T TpI_{equi} to the first excited state is not expected to lead to the formation of 2AP–T TpII in the excited state.

In summary, the potential energy curves found in this work have enabled the identification of stable ground state (S_0) and first electronic excited state (S_1) base pair tautomers for PC–G and 2AP–T and suggest, in the case of PC–G, that excited state conversion of tautomeric forms may occur, allowing potentially for alternative decay pathways when PC is in a hydrogen bonded environment with guanine.

Supporting Information

Ground State (S_0) PC–G Potential Energy Curves (Solution Phase), Ground State (S_0) PC–G $TpII_{equi}$ Structure (Solution Phase), Excited State (S_1) PC–G Potential Energy Curves (Solution Phase), PC–G $TpII_{equi}$ Structure in Electronically Excited States (Solution Phase), Ground State (S_0) 2AP–T Potential Energy Curves (Solution Phase), Excited State (S_1) 2AP–T Potential Energy Curves (Solution Phase), and 2AP-T $TpII_{equi}$ Structure in Electronically Excited States (Solution Phase).

AUTHOR INFORMATION

Corresponding Author

*E-mail: k.thompson@mail.cryst.bbk.ac.uk

Notes

The authors declare no competing financial interest.

ACKNOWLEDGEMENTS

The authors wish to thank Dr David Houldershaw for supporting the Asgard cluster at Birkbeck.

REFERENCES

(1) Serrano-Andrés, L.; Merchán, M. (2009) Are the Five Natural DNA/RNA Base Monomers a Good Choice from Natural Selection? A Photochemical Perspective. *Journal of Photochemistry and Photobiology C-Photochemistry Reviews 10***,** 21-32.

(2) Häupl, T.; Windolph, C.; Jochum, T.; Brede, O.; Hermann, R. (1997) Picosecond Fluorescence of Nucleic Acid Bases. *Chemical Physics Letters 280*, 520-524.

(3) Rist, M. J.; Marino, J. P. (2002) Fluorescent Nucleotide Base Analogs as Probes of Nucleic Acid Structure, Dynamics and Interactions. *Current Organic Chemistry 6*, 775-793.

(4) Xu, W.; Chan, K. M.; Kool, E. T. (2017) Fluorescent nucleobases as tools for studying DNA and RNA. *Nature Chemistry 9*,1043–1055.

(5) Ward, D. C.; Reich, E.; Stryer, L. (1969) Fluorescence Studies of Nucleotides and Polynucleotides. I. Formycin, 2-Aminopurine Riboside, 2,6-Diaminopurine Riboside, and Their Derivatives. *The Journal of Biological Chemistry 244*, 1228-1237.

(6) Sowers, L. C.; Boulard, Y.; Fazakerley, G. V. (2000) Multiple Structures for the 2-Aminopurine-Cytosine Mispair. *Biochemistry 39*, 7613-7620.

(7) Eritja, R.; Kaplan, B. E.; Mhaskar, D.; Sowers, L. C.; Petruska, J.; Goodman, M. F. (1986) Synthesis and Properties of Defined DNA Oligomers Containing Base Mispairs Involving 2-Aminopurine. *Nucleic Acids Research 14*, 5869-5884.

(8) Nordlund, T. M.; Andersson, S.; Nilsson, L.; Rigler, R.; Gräslund, A.; Mclaughlin, L. W. (1989) Structure and Dynamics of a Fluorescent DNA Oligomer Containing the *Eco*RI Recognition Sequence: Fluorescence, Molecular Dynamics, and NMR Studies. *Biochemistry 28,* 9095-9103.

(9) Ronen, A. (1979) 2-Aminopurine. *Mutation Research, 75,* 1-47.

(10) Neely, R. K.; Magennis, S. W.; Dryden, D. T. F.; Jones, A. C. (2004) Evidence of Tautomerism in 2-Aminopurine from Fluorescence Lifetime Measurements. *Journal of Physical Chemistry B 108,* 17606-17610.

(11) Smagowicz, J.; Wierzchowski, K. L. (1974) Lowest Excited States of 2-Aminopurine. *Journal of Luminescence 8,* 210-232.

(12) Voet, D.; Gratzer, W. B.; Cox, R. A.; Doty, P. (1963) Absorption Spectra of Nucleotides, Polynucleotides, and Nucleic Acids in the Far Ultraviolet. *Biopolymers 1,* 193-208.

(13) Holmén, A.; Norden, B.; Albinsson, B. (1997) Electronic Transition Moments of 2-Aminopurine. *Journal of the American Chemical Society 119*, 3114-3121.

(14) Rachofsky, E. L.; Osman, R.; Ross, J. B. A. (2001a) Probing Structure and Dynamics of DNA with 2-Aminopurine: Effects of Local Environment on Fluorescence. *Biochemistry 40,*

946-956.

(15) Hardman, S. J. O.; Thompson, K. C. (2006) Influence of Base Stacking and Hydrogen Bonding on the Fluorescence of 2-Aminopurine and Pyrrolocytosine in Nucleic Acids. *Biochemistry 45,* 9145-9155.

(16) Li, S.; Liu, C.; Gong, H.; Chen, C.; Chen, X.; Cai, C. (2018) Simple G-quadruplex-based 2-aminopurine fluorescence probe for highly sensitive and amplified detection of microRNA-21. *Talanta 178,* 974–979.

(17) Rigo, R.; Sissi, C. (2017) Characterization of G4–G4 Crosstalk in the c-KIT Promoter Region. *Biochemistry 56,* 4309–4312.

(18) Zhou, W.; Ding, J.; Liu, J. (2016) A highly specific sodium aptamer probed by 2-aminopurine for robust Na +sensing. *Nucleic Acids Research 44,* 10377–10385.

(19) Pal, S. K.; Zhao, L.; Xia, T. B.; Zewail, A. H. (2003) Site- and Sequence-Selective Ultrafast Hydration of DNA. *Proceedings of the National Academy of Sciences of the United States of America 100,* 13746-13751.

(20) Hochstrasser, R. A.; Carver, T. E.; Sowers, L. C.; Millar, D. P. (1994) Melting of a DNA Helix Terminus within the Active Site of a DNA Polymerase. *Biochemistry*, 33, 11971-11979.

(21) Rachofsky, E. L.; Seibert, E.; Stivers, J. T.; Osman, R.; Ross, J. B. A. (2001b) Conformation and Dynamics of Abasic Sites in DNA Investigated by Time-Resolved Fluorescence of 2-Aminopurine. *Biochemistry 40*, 957-967.

(22) Johnson, N. P.; Baase, W. A.; Von Hippel, P. H. (2004) Low-Energy Circular Dichroism of 2-Aminopurine Dinucleotide as a Probe of Local Conformation of DNA and RNA. *Proceedings of the National Academy of Sciences of the United States of America 101,* 3426-3431.

(23) Guest, C. R.; Hochstrasser, R. A.; Sowers, L. C.; Millar, D. P. (1991) Dynamics of Mismatched Base-Pairs in DNA. *Biochemistry 30,* 3271-3279.

(24) O'Neill, M. A.; Barton, J. K. (2002) 2-Aminopurine: A Probe of Structural Dynamics and Charge Transfer in DNA and DNA : RNA Hybrids. *Journal of the American Chemical Society 124,* 13053-13066.

(25) Berry, D. A.; Jung, K. Y.; Wise, D. S.; Sercel, A. D.; Pearson, W. H.; Mackie, H.; Randolph, J. B.; Somers, R. L. (2004) Pyrrolo-dC and Pyrrolo-C: Fluorescent Analogs of Cytidine and 2 '-Deoxycytidine for the Study of Oligonucleotides. *Tetrahedron Letters 45,* 2457-2461.

(26) Tinsley, R. A.; Walter, N. G. (2006) Pyrrolo-C as a Fluorescent Probe for Monitoring RNA Secondary Structure Formation. *RNA-A Publication of the RNA Society 12,* 522-529.

(27) Fujikawa, M.; Kobayashi, K.; Kozawa, T. (2015) Redox-Dependent DNA Distortion in a SoxR Protein-Promoter Complex Studied Using Fluorescent Probes. *Journal of Biochemistry 157,* 389-397.

(28) Neelakandan, P. P.; Mccullagh, M.; Schatz, G. C.; Lewis, F. D. (2012) Electronic Interactions in Helical Stacked Arrays of the Modified DNA Base Pyrrolocytosine. *Journal of Physical Chemistry B 116*, 5199-5204.

(29) Hardman, S. J. O.; Botchway, S. W.; Thompson, K. C. (2008) Evidence for a Nonbase Stacking Effect for the Environment-Sensitive Fluorescent Base Pyrrolocytosine-Comparison with 2-Aminopurine. *Photochemistry and Photobiology 84,* 1473-1479.

(30) Taherpour, S.; Löennberg, T. (2015) Fluorescence Probing of Metal-Ion-Mediated Hybridization of Oligonucleotides. *RSC Advances 5*, 10837-10844 and Taylor, C. A.; El-Bayoumi, M. A.; Kasha, M. (1969) Excited-State Two-Proton Tautomerism in Hydrogen-Bonded N-Heterocyclic Base Pairs. *Proceedings of the National Academy of Sciences of the United States of America 63*, 253-260.

(31) Zagorskaitė, E.; Sasnauskas, G. (2014) Chemical Display of Pyrimidine Bases Flipped Out by Modification-Dependent Restriction Endonucleases of MspJI and PvuRts1I Families. *PLoS ONE 9*: e114580. doi:10.1371/journal.pone.0114580

(32) Kuznetsov, N. A.; Vorobjev, Y. N.; Krasnoperov, L. N.; Fedorova, O. S. (2012) Thermodynamics of the Multi-Stage DNA Lesion Recognition and Repair by Formamidopyrimidine-DNA Glycosylase Using Pyrrolocytosine Fluorescence-Stopped-Flow Pre-Steady-State Kinetics. *Nucleic Acids Research 40,* 7384-7392.

(33) Kobayashi, K. (2017) Sensing Mechanisms in the Redox-Regulated, [2Fe–2S] Cluster-Containing, Bacterial Transcriptional Factor SoxR. *Accounts of Chemical Research 50*, 1672–1678.

(34) Torres, A. G.; Fabani, M. M.; Vigorito, E.; Williams, D.; Al-Obaidi, N.; Wojciechowski, F.; Hudson, R. H. E.; Seitz, O.; Gait, M. J. (2012) Chemical Structure Requirements and Cellular

Targeting of MicroRNA-122 by Peptide Nucleic Acids Anti-miRs. *Nucleic Acids Research, 40,* 2152-2167.

(35) Hu, X. B.; Li, H. R.; Liang, W. C.; Han, S. J. (2005) Systematic Study of the Tautomerism of Uracil Induced by Proton Transfer. Exploration of Water Stabilization and Mutagenicity. *Journal of Physical Chemistry B 109,* 5935-5944.

(36) Hardman, S. J. O.; Thompson K. C. (2007) The fluorescence transition of 2- aminopurine in double- and single- stranded DNA. *International Journal of Quantum Chemistry 107*, 2092–2099.

(37) Smith, D. A.; Holroyd, L. F.; van Mourik, T.; Jones, A. C. (2016) A DFT study of 2-aminopurine-containing dinucleotides: prediction of stacked conformations with B-DNA structure. *Physical Chemistry Chemical Physics, 18*, 14691–700.

(38) Liang, J.; Matsika, S. (2011) Pathways for Fluorescence Quenching in 2-Aminopurine π -Stacked with Pyrimidine Nucleobases. *Journal of the American Chemical Society 133*, 6799–6808.

(39) Liang, J.; Nguyen, Q. L.; Matsika, S. (2013) Exciplexes and conical intersections lead to fluorescence quenching in π -stacked dimers of 2-aminopurine with natural purine nucleobases. *Photochemical & Photobiological Sciences 12,* 1387-1400.

(40) Perun, S.; Sobolewski, A. L.; Domcke, W. (2006a.) Ab initio studies of the photophysics of 2-aminopurine, *Molecular Physics 104,* 1113-1121.

(41) Thompson, K. C.; Miyake, N. (2005) Properties of a New Fluorescent Cytosine Analogue, Pyrrolocytosine. *Journal of Physical Chemistry* B 109, 6012-6019.

(42) Dreuw, A.; Head-Gordon, M. (2004) Failure of Time-Dependent Density Functional Theory for Long-Range Charge-Transfer Excited States: The Zincbacteriochlorin-Bacteriochlorin and Bacteriochlorophyll-Spheroidene Complexes. *Journal of the American Chemical Society, 126,* 4007-4016.

(43) Yamazaki, S.; Taketsugu, T. (2012) Photoreaction Channels of the Guanine-Cytosine Base Pair Explored by Long-Range Corrected TDDFT Calculations. *Physical Chemistry Chemical Physics 14,* 8866-8877.

(43) Broo, A.; Holmen, A. (1997) Calculations and Characterization of the Electronic Spectra of DNA Bases Based on *ab Initio* MP2 Geometries of Different Tautomeric Forms. *Journal of*

Physical Chemistry A 101, 3589-3600.

(44) Frisch, M. J.; Trucks, G. W.; Schlegel, H. B.; Scuseria, G. E.; Robb, M. A.; Cheeseman, J. R.; Montgomery, J. A. Jr.; Vreven, T.; Kudin, K. N.; Burant, J. C.; Millam, J. M.; Iyengar, S. S.; Tomasi, J. J.; Barone, V.; Mennucci, B.; Cossi, M.; Scalmani, G.; Rega, N.; Petersson, G. A.; Nakatsuji, H.; Hada, M.; Ehara, M.; Toyota, K.; Fukuda, R.; Hasegawa, J.; Ishida, M.; Nakajima, T.; Honda, Y.; Kitao, O.; Nakai, H.; Klene, M.; Li, X.; Knox, J. E.; Hratchian, H. P.; Cross, J. B.; Bakken, V.; Adamo, C.; Jaramillo, J.; Gomperts, R.; Stratmann, R. E.; Yazyev, O.; Austin, A. J.; Cammi, R.; Pomelli, C.; Ochterski, J. W.; Ayala, P. Y.; Morokuma, K.; Voth, G. A.; Salvador, P.; Dannenberg, J. J.; Zakrzewski, V. G.; Dapprich, S.; Daniels, A. D.; Strain, M. C.; Farkas, O.; Malick, D. K.; Rabuck, A. D.; Raghavachari, K.; Foresman, J. B.; Ortiz, J. V.; Cui, Q.; Baboul, A. G.; Clifford, S.; Cioslowski, J.; Stefanov, B. B.; Liu, G.; Liashenko, A.; Piskorz, P.; Komaromi, I.; Martin, R. L.; Fox, D. J.; Keith, T.; Al-Laham, M. A.; Peng, C. Y.; Nanayakkara, A.; Challacombe, M.; Gill, P. M. W.; Johnson, B.; Chen, W.; Wong, M. W.; Gonzalez, C.; Pople, J. A.; (2003) *Gaussian 03*, revision E.01, Gaussian, Inc., Wallingford CT, 2004.

(45) Flükiger, P.; Lüthi, H. P.; Portmann, S.; Weber, J. (2002) MOLEKEL 4.3, Swiss Center for Scientific Computing, Manno (Switzerland).

(46) Miertuš, S.; Scrocco, E.; Tomasi, J. (1981) Electrostatic Interaction of a Solute with a Continuum. A Direct Utilization of Ab Initio Molecular Potentials for the Prevision of Solvent Effects. *Chemical Physics 55,* 117-129.

(47) Miertuš, S.; Tomasi, J. (1982) Approximate Evaluations of the Electrostatic Free Energy and Internal Energy Changes in Solution Processes. *Chemical Physics 65,* 239-245.

(48) Perun, S.; Sobolewski, A. L.; Domcke, W. (2005) Ab Initio Studies on the Radiationless Decay Mechanisms of the Lowest Excited Singlet States of 9H-Adenine. *Journal of the American Chemical Society 127,* 6257-6265.

(49) Perun, S.; Sobolewski, A. L.; Domcke, W. (2006b) Conical Intersections in Thymine. *Journal of Physical Chemistry A, 110,* 13238-13244.

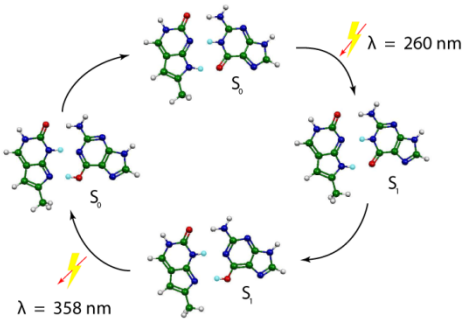

For Table of Contents Only